Electronic Supplementary Material (ESI) for Journal of Materials Chemistry C.

Supplementary Information

Tahere Hemati,† Xintong Zhang,‡ and Binbin Weng*,†

†*School of Electrical & Computer Engineering, University of Oklahoma, Norman, Oklahoma 73019, USA*

‡*School of Physics, Northeast Normal University, Changchun 130024, Jilin, China*

E-mail: binbinweng@ou.edu

IBI-grown Film's Band-gap Simulation

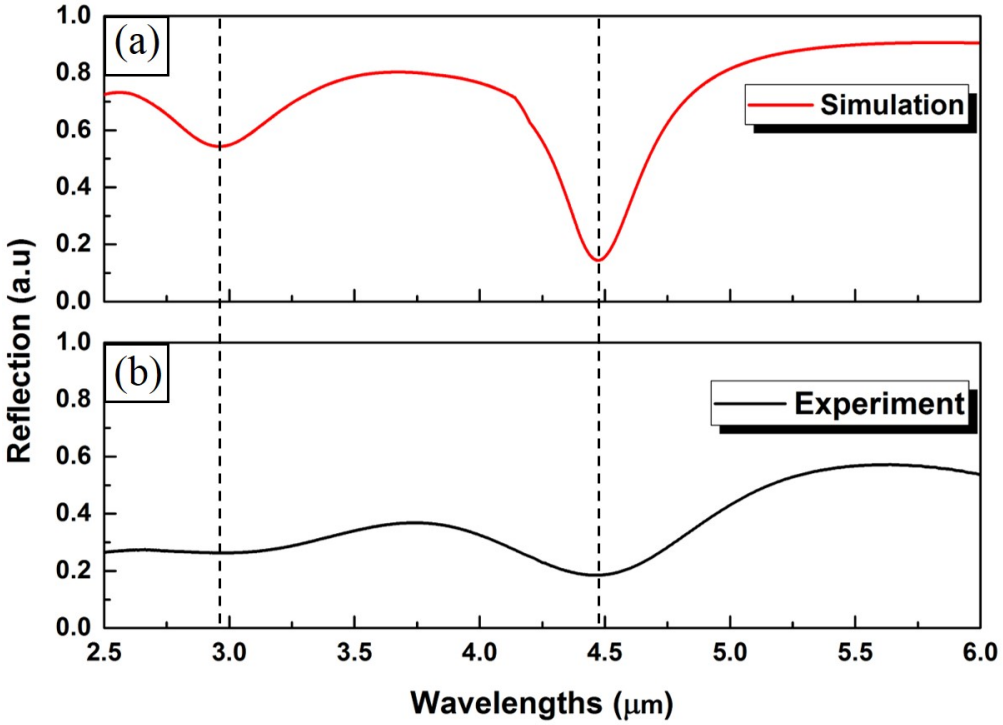

Figure 1: **a)** The reflection of the simulated PbSe with a thickness of 920 nm and the band-gap of 4.4 μm. **b)** The reflection of the IBI-grown PbSe film by FTIR. In both plots (simulation and experiment) the incident angle is 60°.

To make sure about the accuracy of the band-gap calculation, a layer of PbSe with a thickness of 920 nm on the SiO_2 substrate was simulated (the thickness of the substrate was considered infinite). The thickness of the simulated PbSe layer is matched with the thickness of the deposited film. To have a more realistic simulation, the related data-set of bulky PbSe was imported.[1] In this data-set, the band-gap of the PbSe was defined as 4.4 μm. Figure 1.a shows the simulation result of a PbSe layer with thickness of 920 nm and figure 1.b indicates the measured reflection from IBI-grown sample. As we can see, there is a good match between simulation and experiment. Hence, the position of the simulated reflection valleys is matched with the reflection valleys of the experiment. Since the simulated sample band-gap is 4.4 μm, and the IBI deposited film shows the same pattern with the same valleys' position, we expect that the IBI-grown film band-gap would be around 4.4 μm.

Preparation Temperature

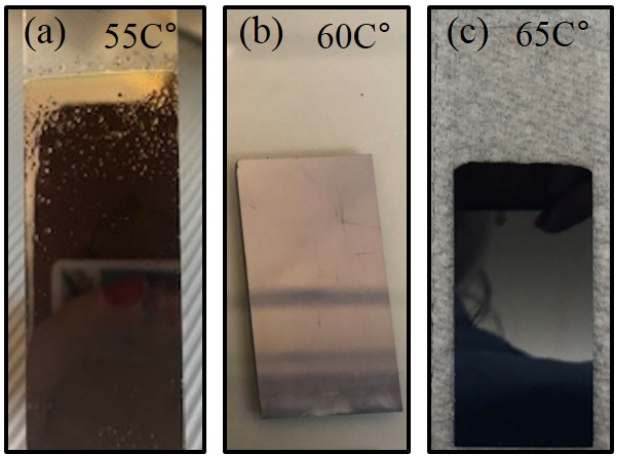

Figure 2: A picture of the film deposited at 45°C, pH 9.8, for ten minutes when the preparation temperature is **a)** 55°C; **b)** 60°C, and **c)** 65°C.

Size-tunability

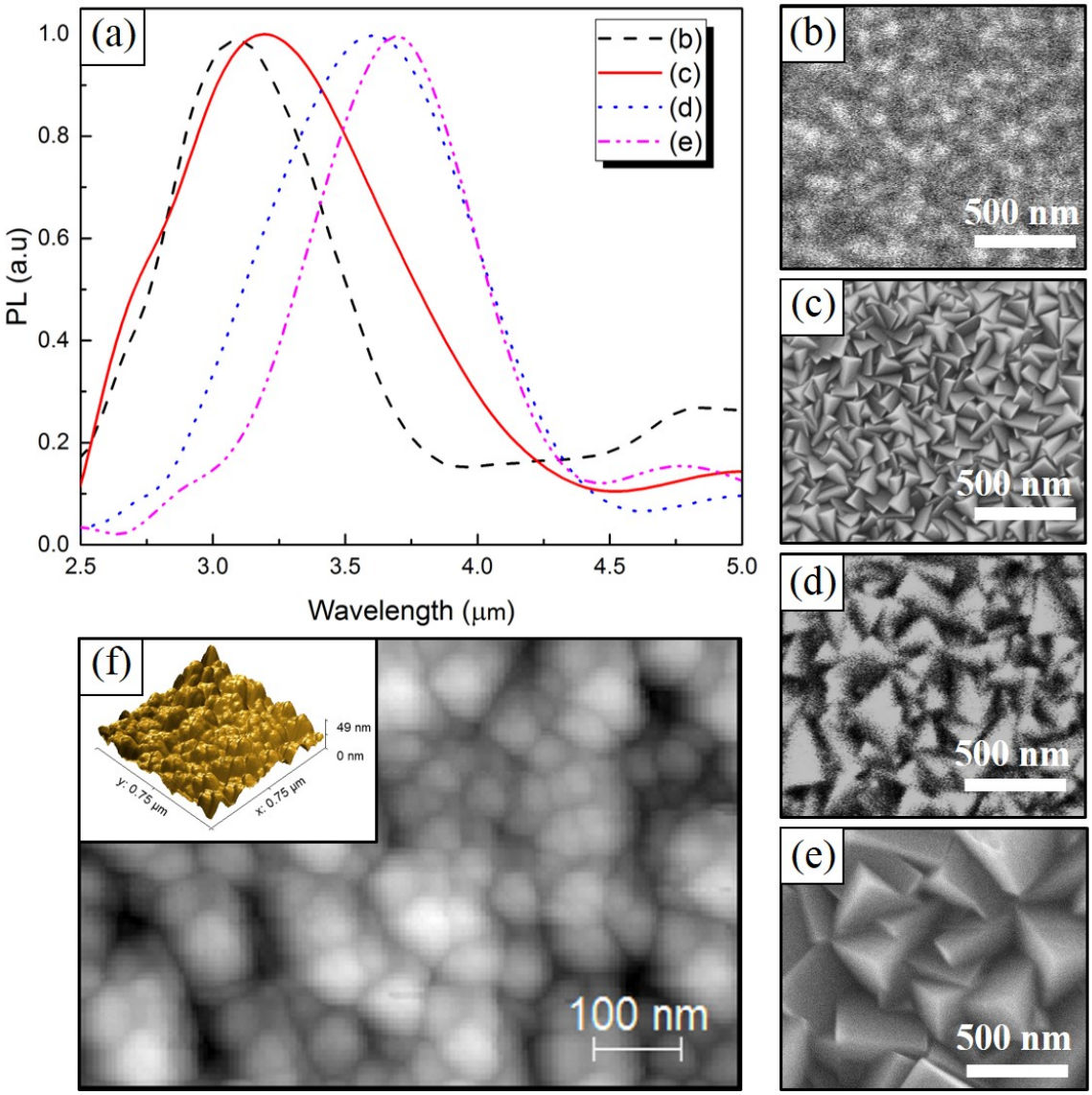

Figure 3: **a)** The normalized PL spectra of the samples, deposited at 40°C, pH∼9.7, for ten minutes prepared at different temperatures. SEM imaging of the deposited film, when the preparation temperature is **b)** 45°C; **c)** 55°C; **d)** 65°C; **e)** 75°C. **f)** The AFM imaging of sample (c). Inset shows a 3D view of the surface roughens of sample (c).

Figure 3.a shows the PL-tunability of the deposited films, prepared at different temperatures. The SEM imaging of these films is shown, as well. Moreover, figure 3.f indicates the AFM image of sample (c). From this photo is evident that each pyramidal-shape grain (size $\sim$ 100 nm) is composed of smaller agglomerated crystals (size $\sim$ 25 nm). Furthermore,

inset shows a 3D view of the sample (c) taken on 0.75×0.75 μm^2 surface. The given RMS roughness of this sample is 7.71 nm.

X-Ray Photoelectron Spectroscopy (XPS)

To study the deposited films' air stability and oxidation process in more detail, we performed the X-Ray Photoelectron Spectroscopy (XPS) on the the surface of IBI, OA, and cluster grown films. The XPS spectra are presented in figure 4 below. Figures 4.(a), (b), and (c) show O 1s core-level spectra of the IBI, OA, and cluster grown films, respectively. Red and black dashed lines are used to help compare the peak position difference.

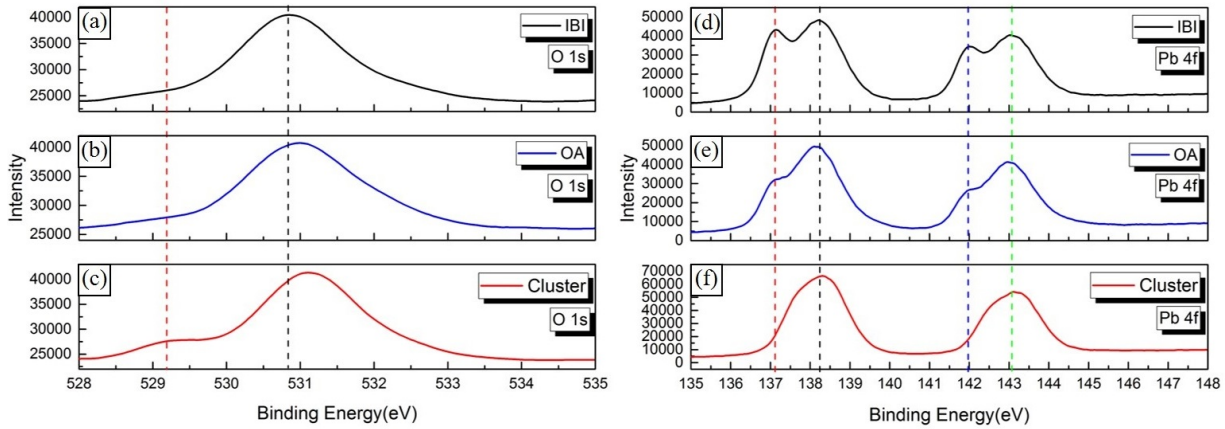

Figure 4: **a)-c)** The XPS spectra of O 1s core-level of the IBI-grown, OA-grown, and cluster-grown samples, respectively; **d)-f)** The XPS spectra of Pb 4f core-level of the IBI-grown, OA-grown, and cluster-grown samples, respectively.

First, a peak around 531 eV can be strongly visualized, which is believed to originate from hydroxide.[2–4] Using the black dashed line as a reference, a distinguishable shift towards higher binding energies is observed from the IBI to the cluster mechanism in a way that the cluster related peak located at the highest binding energy. This shift indicates an increase of hydroxide relative to PbSe. Hence, the IBI deposited film shows the lowest hydroxide/PbSe, while this ratio increased slightly in the OA mechanism and reached its highest amount in the cluster mechanism. In addition, a weak peak located at lower binding energy (BE)

(529.2 eV) is distinct solely in the cluster-grown film. Since this peak often attributed to the existence of lead oxide,[2,5–7] the oxide reaction is more considerable in the cluster growth than in the OA and IBI processes.

Besides, figures 1(d), (e), and (f) are the Pb 4f core-level spectra of the IBI, OA, and cluster grown films, respectively. The red, black, blue, and green dashed lines are used to help compare the peak position difference. The XPS spectrum of the IBI film (figure 4(d)), is dominated by two doublet peaks. The first doublet peak located at lower BE is associated with $4f_{5/2}$ spin-orbit, and the second one located at higher BE arises from $4f_{7/2}$ spin-orbit of Pb.[8] Since the higher BE Pb peak in each doublet band is assumed to be bonded to O or C,[9] they are suggested to be related to the Pb-O adducts in the form of lead oxide, lead hydroxide, or their combination.[8,9] Further, due to the lower binding energy of PbSe compared to Pb-O or Pb-OH, the lower-energy features (137.1 and 142 eV) are assigned to Pb in PbSe.[10,11] Thus, the doublet peaks phenomenon can be interpreted as a high PbSe/Pb-O ratio in the OA and IBI sample compared with the cluster one.

References

(1) Hemati, T.; Weng, B. Theoretical study of leaky-mode resonant gratings for improving the absorption efficiency of the uncooled mid-infrared photodetectors. *Journal of Applied Physics* **2018**, *124*, 053105.

(2) Peters, J. L.; Van Der Bok, J.; Hofmann, J. P.; Vanmaekelbergh, D. Hybrid Oleate–Iodide Ligand Shell for Air-Stable PbSe Nanocrystals and Superstructures. *Chemistry of Materials* **2019**, *31*, 5808–5815.

(3) Zherebetskyy, D.; Scheele, M.; Zhang, Y.; Bronstein, N.; Thompson, C.; Britt, D.; Salmeron, M.; Alivisatos, P.; Wang, L.-W. Hydroxylation of the surface of PbS nanocrystals passivated with oleic acid. *Science* **2014**, *344*, 1380–1384.

(4) Cao, Y.; Stavrinadis, A.; Lasanta, T.; So, D.; Konstantatos, G. The role of surface passivation for efficient and photostable PbS quantum dot solar cells. *Nature Energy* **2016**, *1*, 1–6.

(5) Maskaeva, L. N.; Yurk, V. M.; Markov, V. F.; Kuznetsov, M. V.; Voronin, V. I.; Muhamediarov, R. D.; Zyrianov, G. V. Composition, structure and functional properties of nanostructured PbSe films deposited using different antioxidants. *Materials Science in Semiconductor Processing* **2020**, *108*, 104867.

(6) Taylor, J. A.; Perry, D. L. An x-ray photoelectron and electron energy loss study of the oxidation of lead. *Journal of Vacuum Science & Technology A: Vacuum, Surfaces, and Films* **1984**, *2*, 771–774.

(7) Baker, J. M.; Johnson, R.; Pollak, R. Surface analysis of rf plasma oxidized In and PbInAu films using ESCA. *Journal of Vacuum Science and Technology* **1979**, *16*, 1534–1541.

(8) Sykora, M.; Koposov, A. Y.; McGuire, J. A.; Schulze, R. K.; Tretiak, O.; Pietryga, J. M.; Klimov, V. I. Effect of air exposure on surface properties, electronic structure, and carrier relaxation in PbSe nanocrystals. *ACS nano* **2010**, *4*, 2021–2034.

(9) Sarkar, S. K.; Kababya, S.; Vega, S.; Cohen, H.; Woicik, J. C.; Frenkel, A. I.; Hodes, G. Effects of solution pH and surface chemistry on the postdeposition growth of chemical bath deposited PbSe nanocrystalline films. *Chemistry of materials* **2007**, *19*, 879–888.

(10) Wang, W.; Geng, Y.; Qian, Y.; Ji, M.; Liu, X. A novel pathway to PbSe nanowires at room temperature. *Advanced Materials* **1998**, *10*, 1479–1481.

(11) Jung, H.; Kuljic, R.; Stroscio, M. A.; Dutta, M. Confinement in PbSe wires grown by rf magnetron sputtering. *Applied Physics Letters* **2010**, *96*, 153106.